Design for Manufacturing, Reliability, and Economics

Team 12

2nd Stage Development of an Autonomous Search and Rescue Unmanned Aerial Vehicle (UAV)

Members:

Matthias Clarke – matthias1.clarke@famu.edu

Devin Justice – dsj14b@my.fsu.edu

Trent Loboda – tl12g@my.fsu.edu

Cody Rochford – ctr12f@my.fsu.edu

Marcus Yarber – marcus1.yarber@famu.edu

Qinggele ‘Gale’ Yu – qy16b@my.fsu.edu

Faculty Advisor:

Dr. Farrukh Alvi

Sponsor:

Northrop Grumman

Instructor:

Dr. Nikhil Gupta

4/7/2017

Table of Contents

Table of Figures

Table of Tables

1.0 Design for Manufacturing

The 2nd stage development of an autonomous search and rescue unmanned aerial vehicle (UAV) included far less manufacturing than the 1st stage development. Thus, this report focuses on minor manufacturing required for the payload delivery mechanism and landing gear modifications. However, a general review of the body manufacturing will be completed. All manufacturing occurred within the planned time period, although closer than expected.

Majority of the aircraft is a standard foam airframe which can easily be purchased for mass production, the full assembly is featured below in Figure 1. The foam airframe had to be modified with servos for the ailerons and for the placement of the front and rear plates to attach carbon fiber arms and the propeller motors.

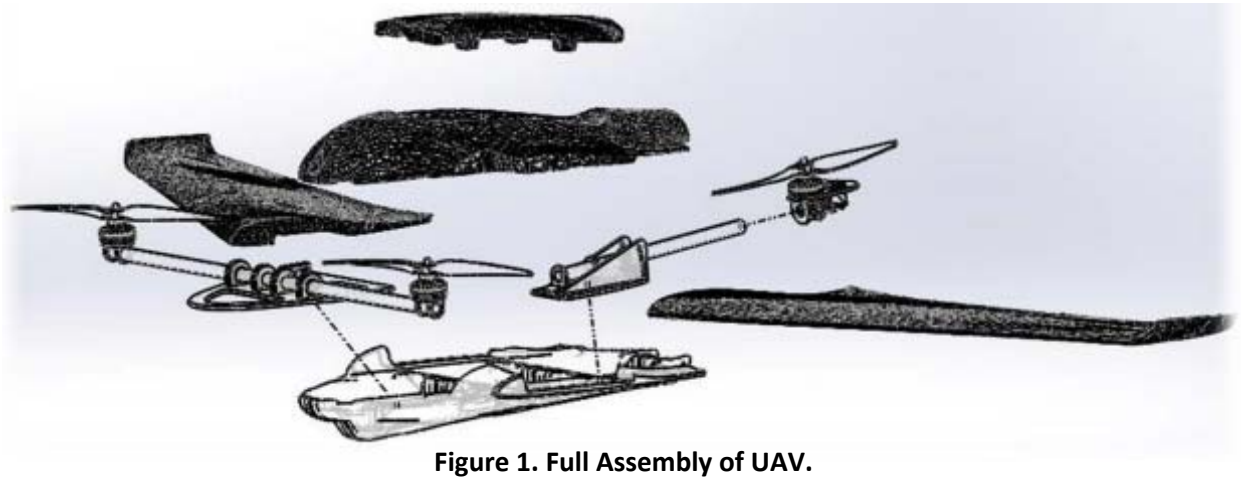

Figure 1. Full Assembly of UAV.

The front and rear plates, featured in Figure 2 and Figure 3 respectively, were manufactured with ABS plastic by use of a laser cutter; this process would be scalable for mass production. Carbon fiber arms were then attached to the frame through the plates and held the propeller motors in position. The carbon fiber arms could be created using carbon fiber prepreg layup methods common in industry or through a vacuum assisted resin transfer molding (VARTM) once a mold was created with plastic, wood, or metal. More likely, carbon fiber tubing is prevalent in the private industry and can be purchased in bulk for an inexpensive total.

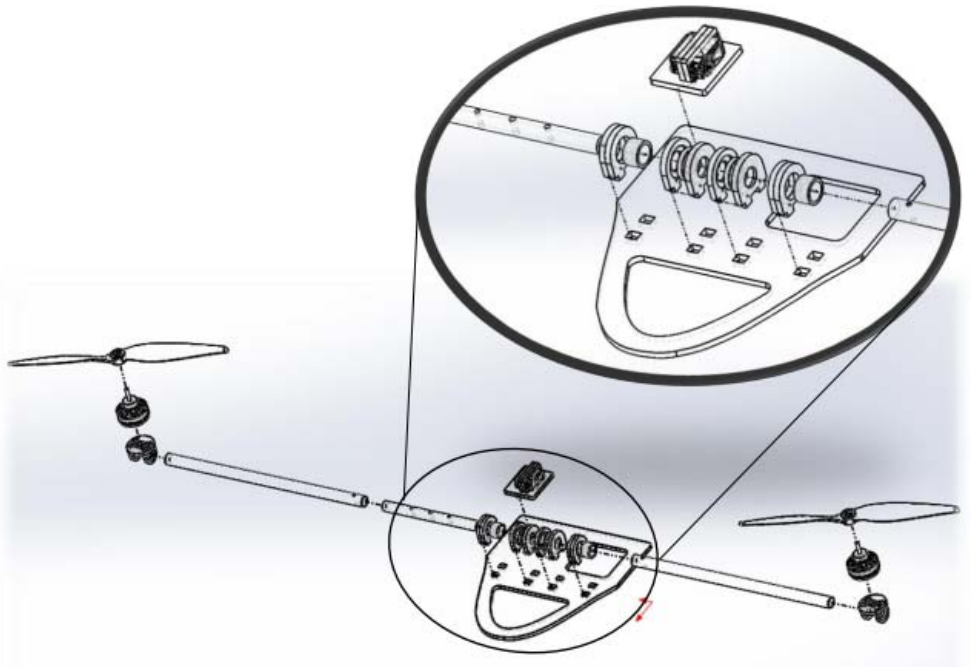

Figure 2. Front ABS Plate.

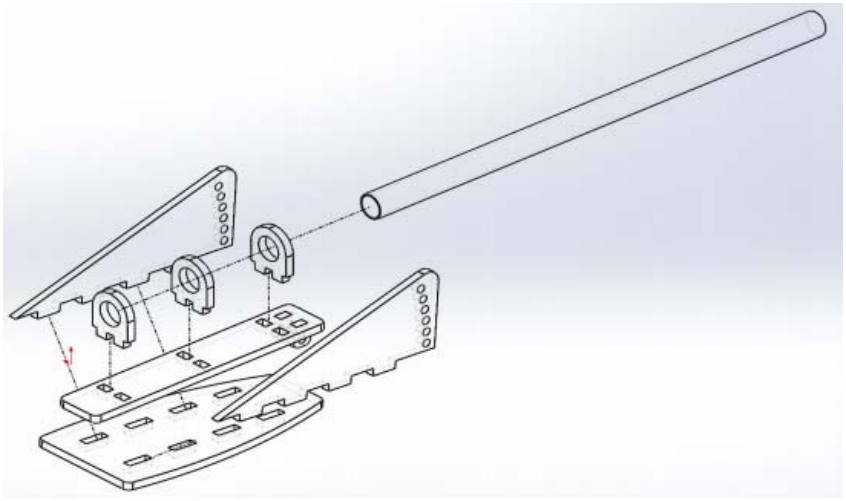

Figure 3. Rear ABS Plate.

All additions made to the UAV were 3D printed ABS material, this was done intentionally to limit cost, weight, and time while encouraging rapid prototyping in order to capitalize on the iterative design process which leads to the best product. Each addition was designed with 3D printing in mind thus high angles were avoided and support material was considered in the design process. First is the payload delivery mechanism which is featured in Figure 4. The mechanism originally contained odd 4 parts including the main housing, the arm, and 2 eyes for the arm to be

attached. To reduce manufacturing loads the eyes were later implemented into the housing to reduce the number of parts to half that of before.

Figure 4. Printed Payload Delivery Mechanism.

The rear landing stilt, designed to allow safe landing conditions by eliminating the possible incidental contact between the front rotors and the ground, was also manufactured using additive manufacturing techniques. The rear landing stilt may be seen below in Figure 5. The stilt was designed to allow quick printing to save time for future iterations, should they be necessary.

Figure 5. Rear Stilt Mount.

2.0 Design for Reliability

Aerodynamic reliability was considered and determined by team 8 last year in the 1st stage of development which included design, manufacturing, and testing of the prototype; further analysis has been completed in the 2nd stage of development including landing load considerations, extended heat exposure, and payload delivery mechanism failure evaluation. The prototype has been determined to be feasible for many uses however would eventually need to have a replaced airframe if used in extreme landing conditions above prescribed flight envelope.

Landing loads were analyzed to determine if failure is possible for the aircraft due to landing. A finite element model was created for the aircraft to ensure no further reinforcement is necessary and to develop the landing flight envelope. Many programs use landing loads as the driving force to the design, this is especially true for aircraft that do not perform dynamic maneuvering and are lightweight. To account for landing gear loads a drop test is typically performed after analysis to ensure structural failure will not occur. The fuselage, in rectangle region of Figure 6, is the section that was analyzed for landing loads effects. This region was selected for its point of contact with the landing gear configuration, thus landing loads will be directly applied to the underside of the fuselage aft of the camera.

Figure 6. Region of Fuselage Analyzed.

The fuselage is a thin walled structure which has been hollowed out for the housing of electronic components, however it was modeled as a plate structure for theoretical calculations performed by hand. In order to further simplify the theoretical solution landing loads will be applied in uniform to the bottom side of the approximated plate; the simplified scenario is featured in Figure 7. Realistically the loads would be applied at the two points of contact, this was implemented in the finite element model but is not necessary in theoretical calculations since they will serve as verification but will not be used in design.

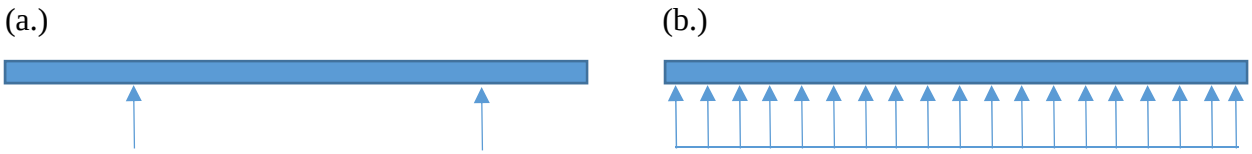

Figure 7. Theoretical Model Calculation Schematic.

In theoretical calculations the boundary conditions were taken as the structure being stationary, this allowed for a simple model which still accurately represented the physical model without unnecessary added complexities. The analysis of the finite element model in relation to the theoretical results are outlined later in this report and will explain why further complexities were not required in the theoretical model. The model was created with rigid polyurethane, and theoretical calculations were conducted using normal stress equations to verify the model. The preliminary finite element model was created as shown in Figure 8, a simple plate was created to represent the lower surface of the fuselage. The upper edge was set to zero displacement as the only boundary condition, ideally the left and right edge would be selected however if so the model

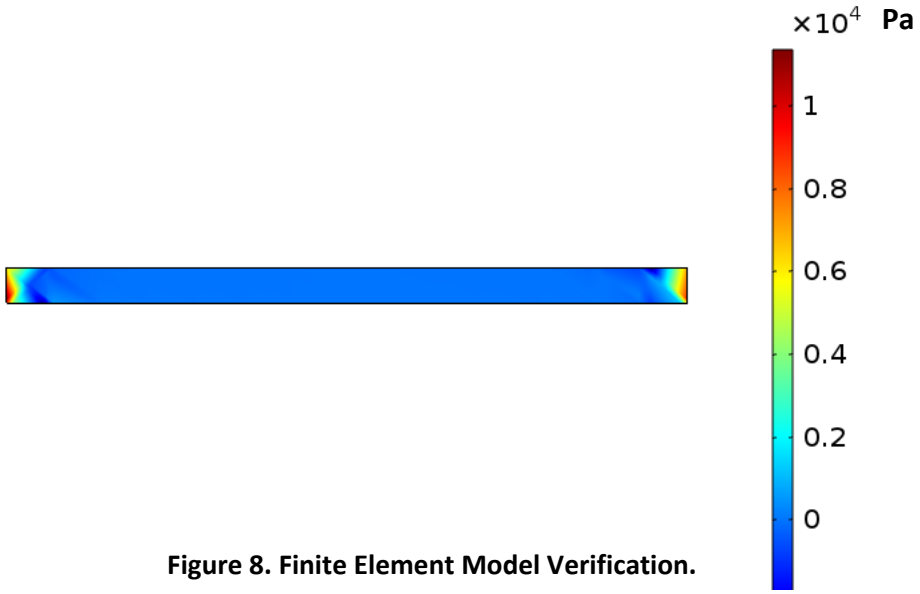

Figure 8. Finite Element Model Verification.

would not generate a stress as the boundary condition conflicts with the force applied. A flux was applied at the lower edge in the positive y direction. When the model was subjected to a force of 51 N, the force achieved with a 3 m/s sink rate, the model yielded a maximum stress of 11 kPa. This simple model was verified with the theoretical calculations described above, thus a plate of equal dimensions was subjected to a uniform force on the lower edge yielding a normal force of approximately 11.16 kPa. The percent error associated with this crude preliminary model is approximately 1.45% hence the model has been deemed acceptable and a more complex and representative geometry was pursued. The model also makes sense intuitively in the sense that the stress concentrations are located on the ends of the structure.

A more complex model was then created which featured the cross section of the fuselage. The model does not fully represent the physical scenario as approximations were implemented in order to create a simpler model that still accurately predicts stress conditions on the structure. First,

plane strain model was utilized since the fuselage cross section dimensions are much less than the dimensions spanning from the fore to the aft of the aircraft. This same approximation is used for long cylinders; such as dams, tunnels, and commercial aircraft cabins. Second, the loads are only applied at the points of contact between the forward landing gear and the fuselage. This approximation was done since the majority of the load would be on the forward wheels rather than the trailing wheel, therefore making the stress exerted on the structure more likely to induce failure. Third, the model geometry does not contain the wing geometry since nearly the entire load shows to dissipate before reaching the edge of the fuselage. This approximation was originally made for simplicity; once the model was completed the rapid dissipation of stress, assumed to be due to poor load transfer, led to the approximation being deemed reasonable. The results of this finite element model are displayed for 51 N of force in Figure 9 along with a section view of the stress concentration.

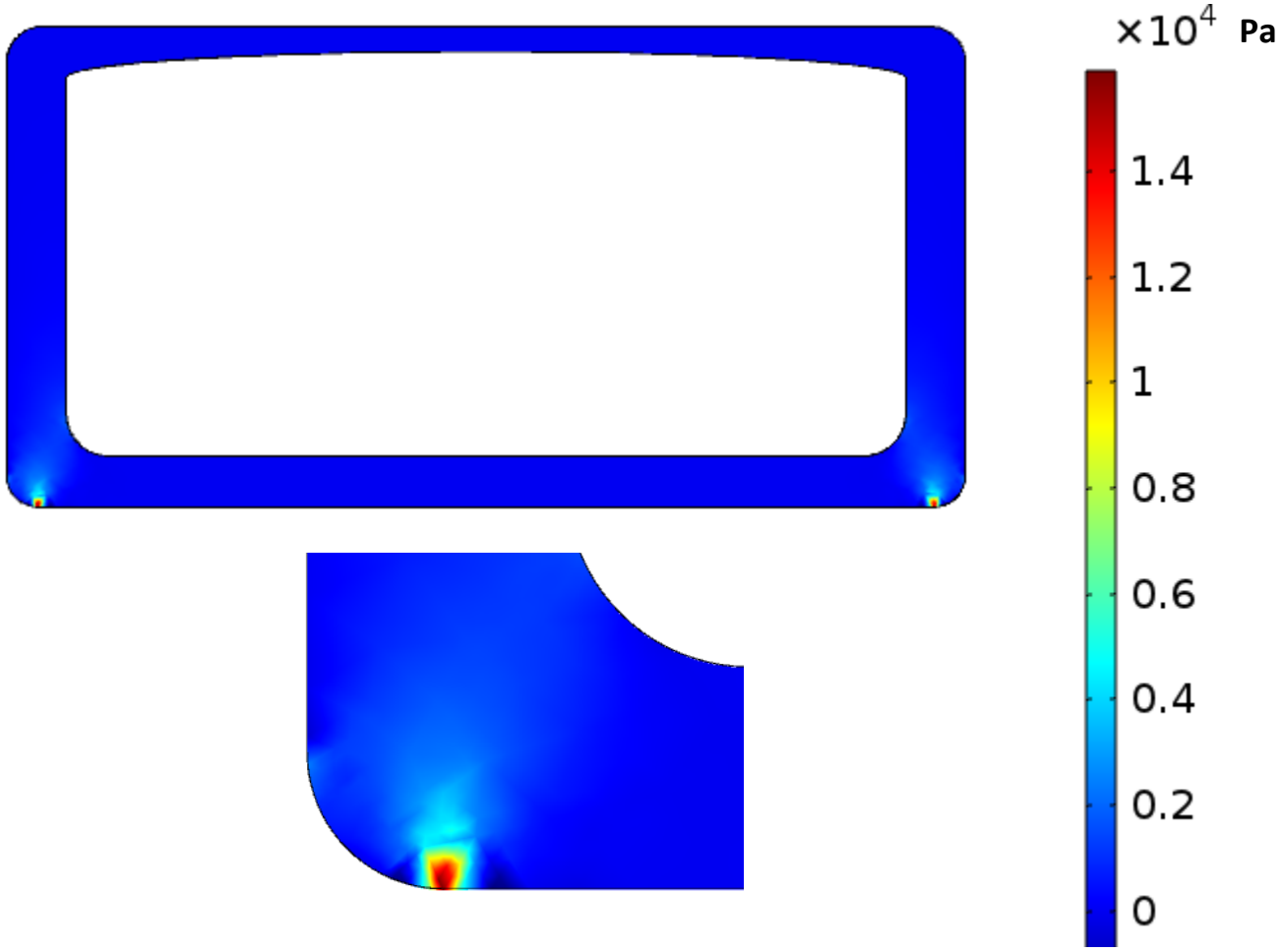

Figure 9. Finite Element Model Results.

In the finite element model above a force was applied at the point of the two stress concentrations, this force was calculated for a sink rate of 3 m/s and yielded a stress of approximately 15 kPa. A second iteration subjected the model to a force of 170 N at 10 m/s sink rate and yielded a maximum stress of approximately 52 kPa.

The maximum stress predicted by the latter model is greater than that calculated theoretically by approximately 34%. Although significantly higher than the theoretical stress, the model stress was determined to be reasonable since the point source of force results in the same force being applied upon a smaller area than that used in theoretical calculations. Thus further analysis using stresses calculated by the model commenced.

Applying various failure criterion to the structure inputting maximum stress from this model predicts that the structure will not fail. Rankine theory, also referred to as maximum-normal stress theory, is a particularly conservative criterion for such cases; applying Rankine theory led to a non-failure evaluation since the maximum stress of 15 kPa for 3 m/s sink rate and 52 kPa for 10 m/s sink rate is much less than the ultimate tensile strength of 79 kPa. However, conservatively it is recommended not to fly at 10 m/s sink rate in order to ensure a 1.5 factor of safety. Iterations were conducted with various loading on a single point as if the aircraft landed at different angles, however none of the stresses induced yielded anything of interest, thus they were not explored further at this point.

Based upon the results yielded by the finite element model outlined in this report no further action must be taken in reinforcing the current aircraft structure in preparation of landing loads. Further analysis may be conducted in the future to account for any induced vibrations in the thin regions of the wing since failures have occurred in this region occasionally due to other loads, such as wind loads and so forth.

In order to ensure operation at extreme temperature conditions, a peak temperature of 110°F (approximately 316 K) or 100°F (approximately 310 K) over a 12 hour period, a finite element model was created to simulate such conditions. A temperature of 316 K was applied to the exterior of the foam cover shielding the electronic housing from the environment. A transient model was then executed over 12 hours and resulted in minimal risk temperatures thus deeming the aircraft free of overheating issues. The finite element model is featured below in Figure 10.

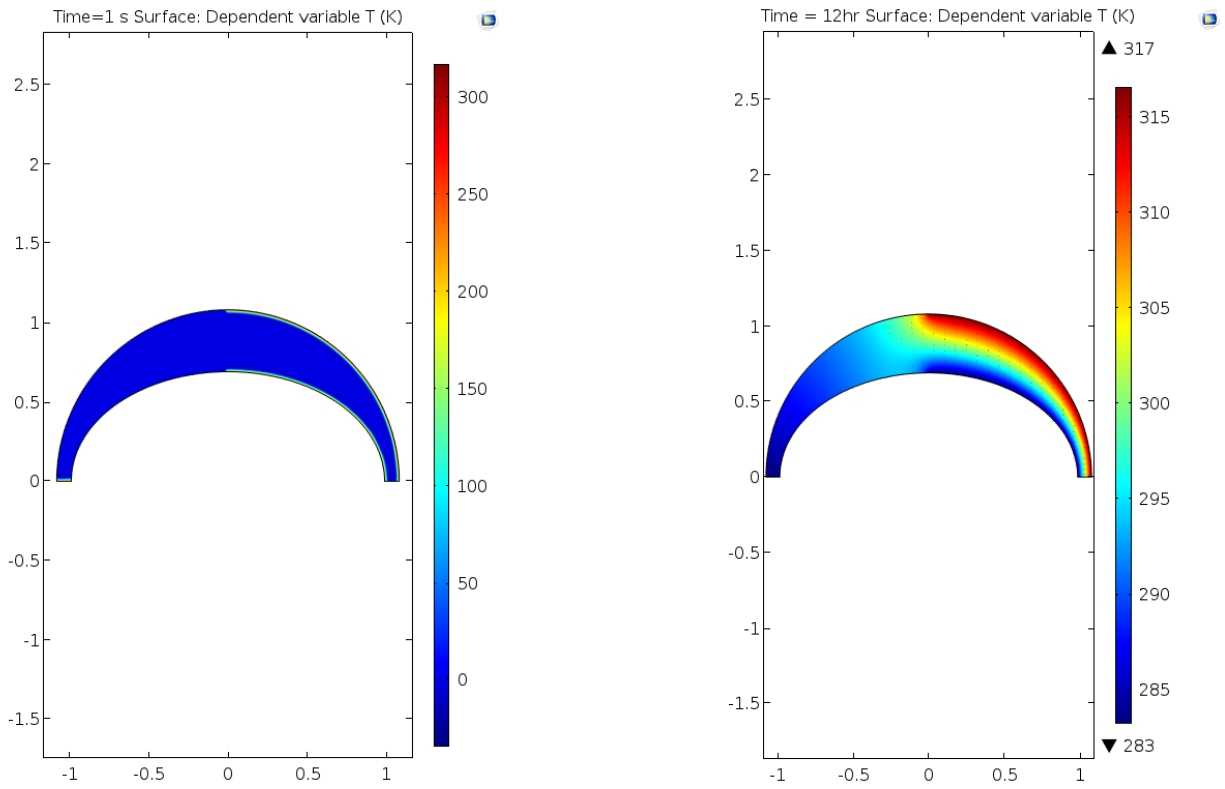

Figure 10. Finite Element Model Transient Heat Transfer Results.

Upon assurance of the aircraft's ability to handle landing induced loads and withstand extreme temperatures under long periods of time, a failure modes and evaluation analysis was conducted of the payload delivery mechanism, seen in Table 1.

Table 1. Failure Modes and Evaluation Analysis of Payload Delivery

Failure	Severity	Occurrence	Detection	RPN
Water bottle falling out	8	3	7	168
Arm jammed with water bottle	5	5	8	200
Arm connection pin/pin slot fracture	8	5	5	200
Parachute deploying during flight	10	3	6	180
Complete mechanism detachment from vehicle	8	4	1	32

It is important to not the most critical failures are the arm jamming with the water bottle and the arm connection failing. Both failures were addressed via in depth testing and iterative design and manufacturing process.

3.0 Design for Economics

The allocated budget for the project is 2,000 dollars. This budget is split into structural modifications, electronic hardware, and a factor of safety of 1.5 was originally implemented. Structural modifications include manufacturing and installment of a payload delivery mechanism which will be 3D printed with ABS, new landing gear, and a spare foam body in case of a failure. Electronics budget is made up of a Zubax GNSS 2, ODROID C2, Ultrasonic sensor, wifi antenna, and a camera system as well as spare electronics in case of failure. Table 2 below features the allocated resources while Figure 11 shows a pie chart visualization of the resource allocation.

Table 2. Resource Allocation

Category	Amount in dollars
Electronic Hardware:	$410.00
Structural Modifications:	$580.00
Total:	**$990.00**

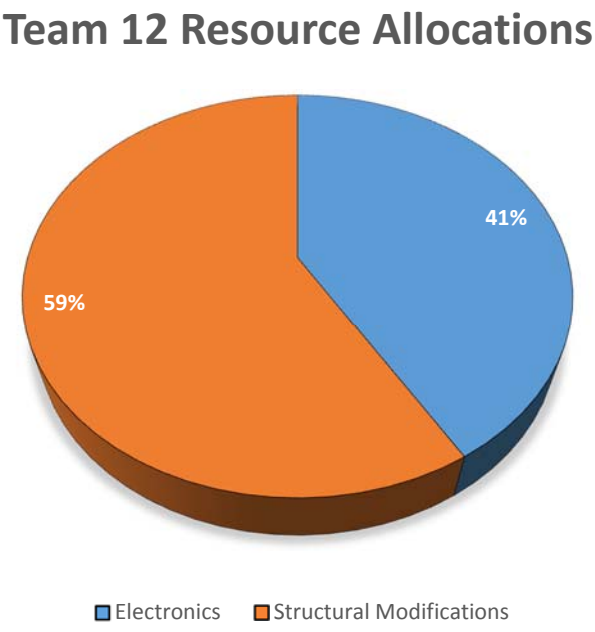

Figure 11. Resource Allocation Categories Pie Chart.

A similar product is currently on the market, in the FireFLY6 which is a vertical takeoff and landing UAV sound in retail for $5,999.00 below in Figure 12.

Figure 12. FireFLY6 UAV.

It is useful to compare said product to our product however certain considerations must be made. First, the FireFLY6 is more dynamic and has higher performance than our product, however our product is smarter in terms of stationary and dynamic target detection software. Furthermore, because this is the 2nd stage of development of our product the 1st stage must also be included when comparing total costs. Therefore, the total cost for the UAV produced by team 8 last year and team 12 this year is $1,771.55. A bar graph comparing the UAV prototype to the FireFLY6 can be found in Figure 13 below.

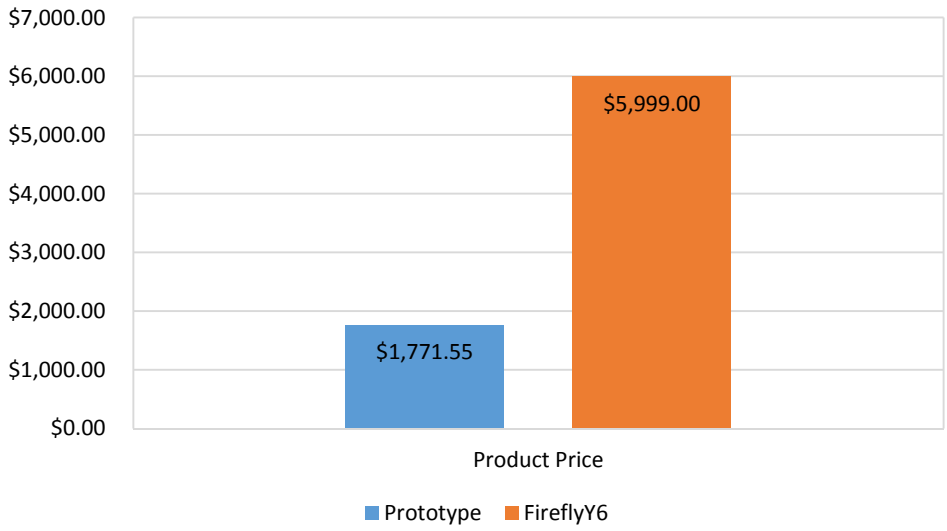

Figure 13. FireflyY6 and Prototype Cost Comparison.

4.0 References

[1] Roland Siegwart, I. R. (2011). Introduction to Autonomous Mobile Robots. Cambridge: The MIT Press.

[2] Lorenz Meier, P. T. (2011). PIXHAWK: A System for Autonomous Flight using Onboard Computer. IEEE International Conference on Robotics and Automation.

[3] Pixhawk Home Page Retrieved from Pixhawk Autopilot: https://pixhawk.org/modules/

[4] Tedrake, A. J. (2015). Pushbroom Stereo for High-Speed Navigation in Cluttered Environments. IEEE International Conference on Robotics and Automation.

[5] Saurabh Ladha, D. K. (n.d.). Use of LIDAR for Obstacle Avoidance by an Autonomous Aerial Vehicle. IEEE Conference on Robotics and Automation.

[6] DJI Phantom 4: Finally an Obstacle-Avoiding, Object-Tracking Quadcopter. (n.d.). Retrieved from Makezine:http://makezine.com/2016/03/01/dji-phantom-4-finally-an-obstacle-avoiding- object-tracking-quadcopter/

[7] Competition Rules SUAS 2017. (2017).

[8] Luber, Wolfgang. "Dynamic Landing Loads on Combat Aircraft with External Stores Using Finite Element Models." *European Aeronautic Defence and Space Company – EADS* Web. 25 Nov. 2016.

[9] Witkiewicz, Wit. "Properties of the Polyurethane (PU) Light Foams." *Advances In Materials Science* 10th ser. 6.2 (2006): Web. 25 Nov. 2016.

[10] Callister, William D. *Materials Science and Engineering: An Introduction*. New York: Wiley, 2000. Print.

[11] Pixy Camera Detect the Colour of the Objects and Track Their Position. (n.d.). Retrieved from OpenElectronics: http://www.open-electronics.org/pixy-camera-detect-the-colour-of-the-objects- and-track-their-position/

[12] Rosebrock, A. (2015, May 4). Target acquired: Finding targets in drone and quadcopter video streams using Python and OpenCV. Retrieved from http://www.pyimagesearch.com/2015/ 05/04/target-acquired-finding-targets-in-drone-and-quadcopter-video-streams-using-python-and- opencv/

[13] Jangwon Lee, J. W. (2015). Real-Time Object Detection for Unmanned Aerial Vehicles based on Cloud-based Convolutional Neural Networks.

[14] K. Senthil Kumar, G. K. (2011). Visual and Thermal Image Fusion for UAV Based Target Tracking . InTech Open.

[15] Oleg A. Yakimenko, E. A. (2015). Autonomous Aerial Payload Delivery System “Blizzard”. 21st AIAA Aerodynamic Decelerator Systems Technology Conference and Seminar. Dublin,Ireland.

[16] Chris Archer, O. Y. (2012). Enhancing SOF through UAV Pinpoint Payload Delivery. SOF Mobile Systems Focus Day. San Diego.

[17] Academy of Model Aeronautics National Model Aircraft Safety Code. (2014, January 1).